Sequential Activation of Molecular Breathing and Bending during Spin-Crossover Photoswitching Revealed by Femtosecond Optical and X-Ray Absorption Spectroscopy

Marco Cammarata, Roman Bertoni, Maciej Lorenc, Hervé Cailleau, Sergio Di Matteo, Cindy Mauriac, Samir Matar, Henrik Lemke, Matthieu Chollet, Sylvain Ravy, et al.

Sequential activation of molecular breathing and bending during spin-crossover photoswitching revealed with femtosecond optical and x-ray absorption spectroscopy

Marco Cammarata,[1] Roman Bertoni,[1] Maciej Lorenc,[1] Hervé Cailleau,[1] Sergio Di Matteo,[1] Cindy Mauriac,[2] Samir Matar,[2] Henrik Lemke,[3] Matthieu Chollet,[3] Sylvain Ravy,[4] Claire Laulhé,[4] Jean-François Létard,[2] Eric Collet,[1,*]

**To whom correspondence should be addressed: eric.collet@univ-rennes1.fr*

[1] *Institut de Physique de Rennes, UMR CNRS 6251Université Rennes 1, 35042 Rennes cedex, France.*
[2] *CNRS, Université de Bordeaux, ICMCB, 87 avenue du Dr. A. Schweitzer, Pessac, 33608 France.*
[3] *LCLS, SLAC National Laboratory, Menlo Park, CA, USA.*
[4] *Synchrotron SOLEIL, L'Orme des Merisiers, Saint Aubin, 91192 Gif-sur-Yvette France.*

We study the basic mechanisms allowing light to photoswitch at molecular scale a spin-crossover material from low- to high-spin state. Combined femtosecond x-ray absorption performed at LCLS X-FEL and optical spectroscopy reveal that the structural stabilization of the photoinduced HS state results from a two step structural trapping. Molecular breathing vibrations are first activated and rapidly damped as part of the energy is sequentially transferred to molecular bending vibrations. During the photoswitching, the system follows a curved trajectory on the potential energy surface.

PACS Codes : 42.70.Gi, 75.30.Wx, 78.47.J-, 82.53.Xa

Introduction.– A wide range of phenomena in matter are driven by changes that occur after illumination with light.[1] This includes chemical, bio-chemical or solid-state reactions,[2,3,4] as well as switching of functionality of materials such as conductivity[5] or magnetism.[6] During a transformation triggered by a femtosecond (fs) laser pulse the excited system is launched onto a complex pathway, from the initial photoexcited to the final photoinduced state, whereby non-equilibrium phenomena, coherent dynamics and interconversion of energy are interconnected.[1] Transition metal complexes undergoing spin-crossover (SCO) from low-spin (LS) to high-spin (HS) state are prototypes of molecular photoswitching in materials.[7] On the shortest time scales the molecule undergoes intersystem crossing (ISC) from the initial photoexcited LS– to HS–state. The structural reorganization of the ligand around the metal centre gives rise to an energy barrier between the trapped HS and the ground LS state. The initial mechanism behind the extremely fast ISC, between states that differ in both spin and structure, defy conventional descriptions. Recent theoretical studies by van Veenendaal[8,9] on ISC in Fe^{II} SCO, mediated by the spin-orbit coupling, discussed the

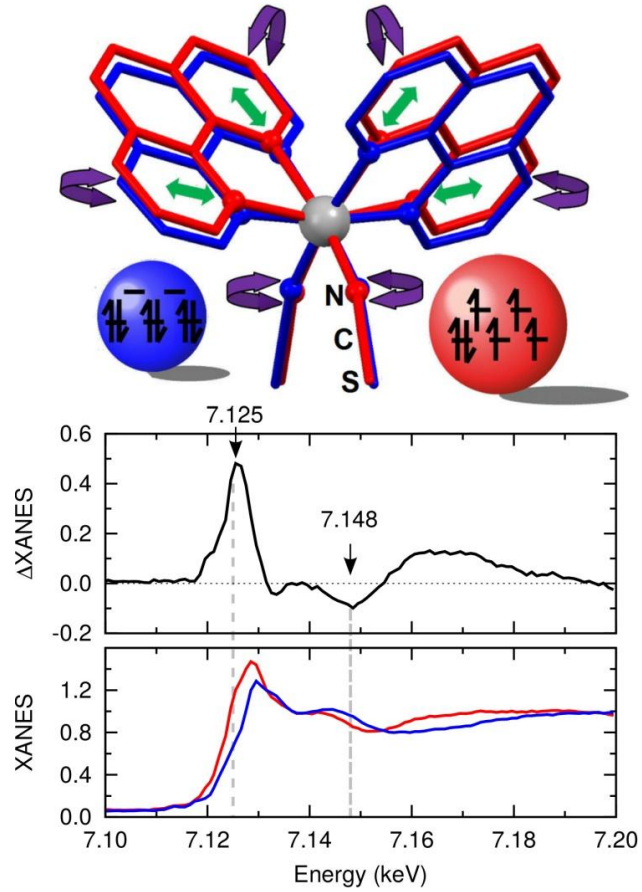

Fig. 1 (color online). (a) LS (140 K, blue) and HS (200 K, red) structures of $[Fe(phen)_2(NCS)_2]$ (phen=1,10-phenanthroline). The central Fe atom is bounded by N to the phenantroline and NCS groups. Green arrows represent the breathing mode and purple ones the bending mode. b) XANES spectra and difference ΔXANES measured between the LS and HS states.

role of significant changes of the metal-ligand distance (molecular breathing). It was proposed that the ultrafast ISC results from the dephasing of the photoexcited state into the HS phonon states. A monotonous decay of the photoexcited state to the HS state becomes efficient when this breathing mode is rapidly damped as energy is dissipated into the environment.

By combining femtosecond x-ray absorption near edge structure (XANES) and optical spectroscopy, we provide an experimental evidence of the ultrafast activation and damping of molecular breathing accompanying the ISC, which were lacking up to now. This process is followed by vibrational cooling in the HS potential observed on the bending mode. With respect to conventional models describing SCO photoswitching in terms of potential energy curve along a single breathing coordinate, our work reveals a more complex reality involving a curved trajectory, along breathing and bending, on a multi-dimensional potential energy surface.

Results.– The SCO $[Fe(phen)_2(NCS)_2]$ crystal investigated here, undergoes a first-order phase transition from LS (S=0, $t_{2g}^6 e_g^0 L^0$) to HS (S=2, $t_{2g}^4 e_g^2 L^0$) states above ≈180 K and exhibits photomagnetism and

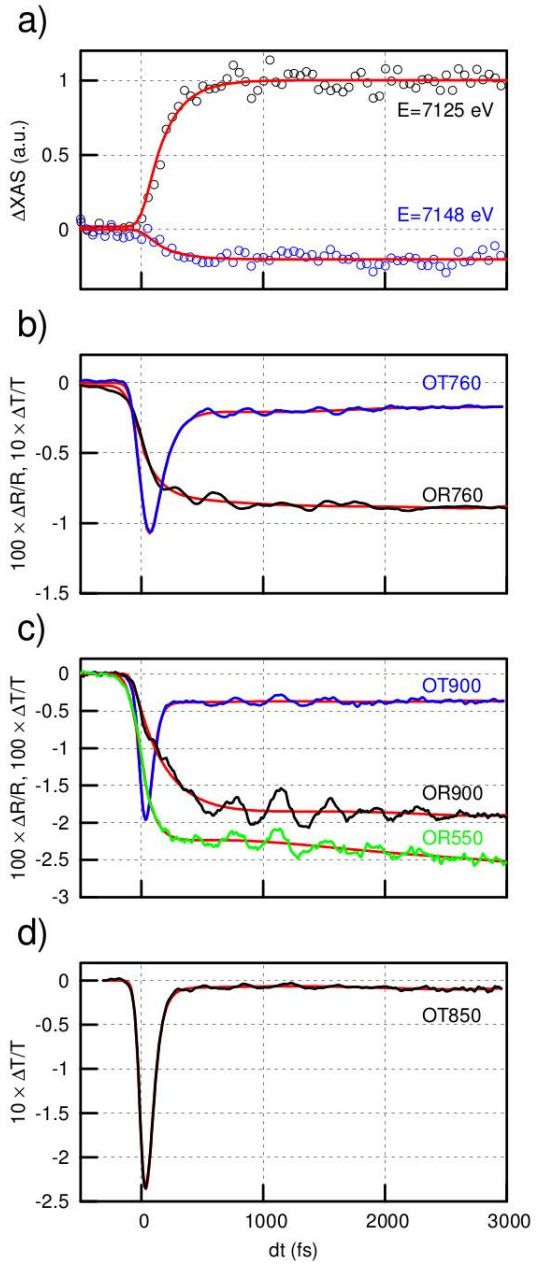

Fig. 2 (color online). Kinetic traces of XANES at 7125 and 7148 eV, fit with a single-exponential function of the rising edge ($\tau_{Fe\text{-}N}$=170 (10) fs) represented by red solid lines (a). Kinetic traces of OR and OT at 760 nm (b), OR at 900 nm & 550 nm and OT at 900 nm (c) and OT 850 nm (d). Fits by a single-exponential function describing the fast change plus a fifth order polynomial are represented by red solid lines.

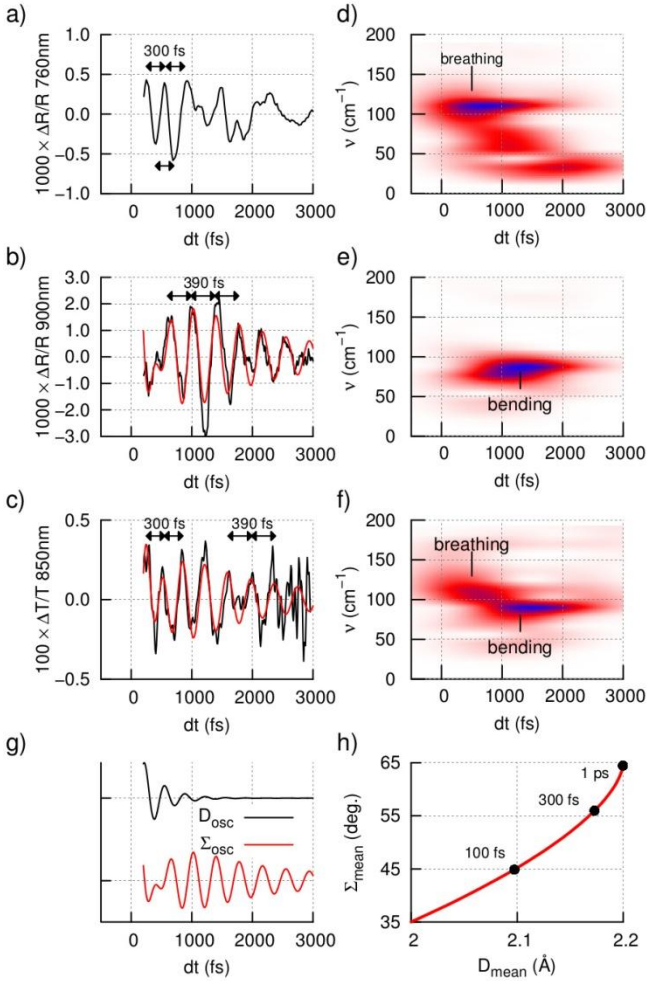

Fig. 3 (color online). (a-c), oscillating component of OR at 760 nm, OR at 900 nm and OT at 850 nm. (d-f), time dependent FFT of the experimental data, showing the activation of the breathing mode and the delayed activation of the bending mode. Combined fits of OR at 900 nm and OT at 850 nm (red line) by the coupled oscillator model, which show the contribution of the bending (Σ) mode (b) and the superposition of bending (Σ) and breathing (D) modes (c). The time course of the oscillating component D_{osc} (300 fs) and Σ_{osc} (390 fs) obtained by the fit in (b) and (c) are displayed in (g) and the average evolutions of D_{mean} and Σ_{mean} obtained by the fit in Fig. 3 are displayed in (h).

photochromism.[7,10,11] Here, *L* corresponds to the LUMO of the ligand. This molecular bi-stability is associated with important structural reorganizations around the FeN_6 octahedron between both spin states (Fig. 1(a), S1 & S2)[12], [131415161718]. The less bonding character of the HS state leads to the expansion of the average Fe-N bond length from $\langle Fe\text{-}N\rangle_{LS}$= 1.97 Å to $\langle Fe\text{-}N\rangle_{HS}$=2.16 Å, often observed for Fe^{II} SCO [7,19]. That changes the XANES spectrum as shown in Fig. 1b, in agreement with the published data on this molecular crystal.[20]

The ultrafast photoswitching dynamics of $[Fe(phen)_2(NCS)_2]$ is investigated in the LS phase at 140 K by two complementary pump-probe methods[12]. A ≈50 fs laser pulse (650 nm) photo-switches LS state to HS via a metal-to-ligand charge-transfer process (MLCT).[10] The changes in XANES are recorded with ≈30 fs x-ray pulses at the XPP station of the LCLS X-FEL,[21] while changes in optical reflectivity (OR) and transmission (OT) are recorded with ≈50 fs VIS-NIR spectroscopy. Fig. 2(a) shows the time course of the XANES signal measured at two energies most sensitive to the structural change (Fig. 1). The increase of XANES signal at 7.125 keV and the decrease at 7.148 keV mainly result from Fe-N elongation[20] and are the fingerprints of the formation of HS structures.

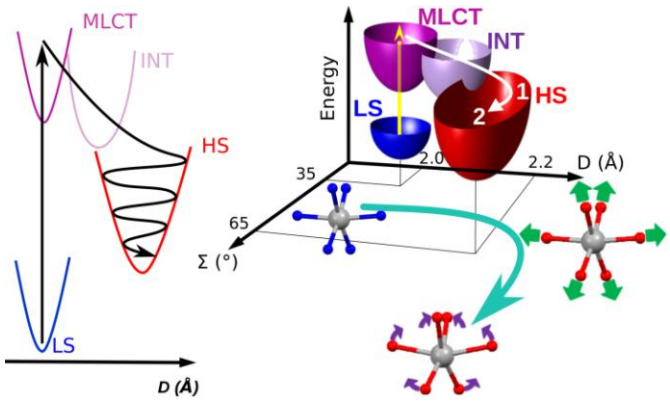

Fig. 4 (color online). (a) schematic representation of the elongation and damping of the breathing mode along the *D* coordinate . (b) Classical trajectory in the (*D*,*Σ*) space. Molecules in the LS (blue) potential reach ^{1}MLCT state by light excitation. Fast ISC, through possible INT states, drives *D* elongation during step 1 with the generation and damping of breathing phonon, followed by activation of additional bending phonons such as distortion *Σ*, during step 2. The sequence is sketched at the bottom.

We fit the rising time by convolving a Gaussian temporal Instrument Response Function (IRF) with an exponential rise ($\tau_{Fe\text{-}N}$). The 110 (10) fs FWHM IRF, obtained by using a timing tool[21] designed to synchronize the optical and the x-ray laser pulses, allows an accurate determination of $\tau_{Fe\text{-}N}$ = 170 (20) fs.

Figs. 2(b-d) & S4 show time traces of OR and OT (with 110 fs IRF) in different spectral zones, revealing two main steps: the onset of OR change or a peak in OT immediately after laser excitation, relaxing towards a plateau during the first 100's fs. The increase of optical absorption on the plateau, which translates into a simultaneous decrease of OR and OT in all probed regions, is another fingerprint of the LS-to-HS photo-switching, also observed during the thermal LS-to-HS conversion[10] (see also Fig. S3). Density of state calculations[22] explain the stronger absorption of the HS state around 760 nm (1.6 eV) by a decrease of the energy gap between t_{2g} and e_g bands from ≈ 1.9 eV (LS) to ≈1.6 eV (HS), due to the molecular ligand field weakening (see also Fig. S5). OT and OR data at 760 nm indicate that the gap narrowing in HS state, resulting from the Fe-N elongation, occurs within $\tau_{Fe\text{-}N}$ = 140 (20) fs. It correlates well with the 170 (20) fs time constant obtained by XANES.

The transient OT peak corresponds to the absorption of the photoexcited singlet ^{1}MLCT state ($t_{2g}^5 e_g^0 L^1$), and other possible intermediate (INT) electronic states[9], and results from transition from a ligand level *L* to higher energy states (see Fig. S5)[10,12]. 760 nm therefore probes both INT and HS (t_{2g}-e_g) absorptions. The t_{2g}-e_g absorption is no more accessible at 850 nm and above, and the main effect in the time traces is the absorption of the INT electronic state. This transient OT peak above 850 nm (Fig. 2(c-d) & S4) better characterizes the depopulation of the INT state, which decays within less than 50 fs. Thus far, our results determine an ISC of tens of fs and a ≈160 fs Fe-N bond elongation in a solid, both of which are similar to those reported for Fe^{II} molecules in solution[23,24,25,26,27,28].

On top of such changes, clear oscillating components are present in the optical data. Fig. 3a-c show the residuals after exponential fit. Data at 760 nm show a coherent vibration around 113 cm^{-1} (≈300 fs oscillation period) in the [0 – 700 fs] range. The corresponding time-dependent Fourier transforms are presented in Fig. 3(d-f) & S4 and the apparent rising time of the 113 cm^{-1} mode is limited by the Gaussian temporal window used[12]. It was already discussed above that OT and OR at 760 nm are sensitive to the Fe-N elongation, hereafter referred to as the breathing coordinate *D*. Therefore, the oscillations riding on 760 nm signals reflect the breathing mode, i.e. the totally symmetric Fe–N stretching, in relation with the symmetry conserving picture of the displacive spin-state switching. This observation is supported by calculations, according to which the only totally symmetric mode (symmetry A in the C_2 point group of the complex) in this frequency range is the breathing mode (≈125 cm^{-1}) in the HS state[29,30]. The breathing mode is represented by green arrows in Fig. 1 and shown in video S1[12]. XANES data do not reveal such small oscillating features after the ≈0.2 Å elongation, because of the noise limit of the measurements, but we underline that the main Fe-N elongation occurs on a timescale approaching the half period of the breathing mode (Fig. 4(a)).

Optical data at 550, 900 nm (Fig. 2(c)) and 950 nm (Fig. S4) reveal another coherent vibration, in-phase for all these probing wavelengths. These oscillations around 85 cm^{-1} correspond to the butterfly mode (also of A symmetry) [29,30], which bends the ligand and the N-Fe-N angles without significantly changing Fe-N distances (see purple arrows in Fig. 1 & video S2). This is a bending coordinate *Σ* [19,31] and such a coherent ligand vibration was also observed for another Fe^{II} SCO molecular system in solution.[26] Unlike the breathing mode, we observed that the bending mode with ≈390 fs period is only activated coherently during a second step, after ≈ 500 fs, with a maximum spectral weight around 1300 fs (Fig. 3 & S4). This bending occurs well after the 160 fs initial Fe-N elongation.

Such oscillations cannot be attributed to impulsive Raman process in the ground LS state because the LS breathing frequency is significantly higher (156 cm^{-1})[29,30]. In addition, there is no optical transitions from LS state to other excited states which can be probed in the 760-950 nm region (Fig. S5) and consequently the LS state is optically silent in our data.

Discussion.– In SCO materials the Fe-N elongations during LS-to-HS conversion are very similar, but the ligand bending *Σ* [12,19,31] also plays an important role for the relative stability of LS and HS states. Hauser evidenced in the kinetic studies of HS→LS relaxation a breakdown of the single mode model and proposed to describe such systems by qualitatively splitting the reaction coordinate into the breathing and the bending modes[32]. Fig. 4(b) is a cartoon of a likely potential energy surface (PES) of $[Fe(phen)_2(NCS)_2]$ in the breathing and bending (*D*,*Σ*) coordinate space. At thermal equilibrium (see ref 13 and Fig. S2) the LS potential is centred at (D_{LS}=1.97 Å, Σ_{LS}=35°) and the one of the HS

state at (D_{HS}=2.16 Å, Σ_{HS}=65°). The delayed activation of the bending Σ, with respect to breathing D is schematically represented in Fig. 4(b) on (D,Σ) PES from stable LS to stable HS locations.

XANES, OT and OR data at 760 nm give an average elongation D_{mean}(t) with a ≈160 fs time constant. OR at 900 nm, no more sensitive to D but only to the change of Σ, gives an average torsion Σ_{mean} *(t)* with 250 fs time constant. We thus deduce from these different breathing and bending timescales a curved trajectory in the relevant coordinate space (D,Σ) on PES. If we simply assume that the photoinduced HS state is not significantly different from the HS structure at thermal equilibrium, we can plot a trajectory in Fig. 3(h). It indicates that around 1 ps the motion is mainly along Σ, also simultaneously manifested by the strong spectral weight of the bending mode (Fig. 3(e-f)). The coupling of instantly photo-activated phonons to other modes can drive major structural reorganization in solids.[4,33,34] In the present case, the energy transfer between the two totally symmetric breathing (D) to bending (Σ) modes can be described by a linear coupling, with the classical equations of motion of coupled harmonic oscillators:

$$\begin{cases} \mu_D \ddot{D} + \gamma_D \dot{D} + k_D D + k_{D\Sigma}(D - \Sigma) = 0 \\ \mu_\Sigma \ddot{\Sigma} + \gamma_\Sigma \dot{\Sigma} + k_\Sigma \Sigma - k_{D\Sigma}(D - \Sigma) = 0 \end{cases}$$

μ_i are the reduced masses of the oscillators (obtained from *Gaussian* calculations[12]), k_i are the force constants refined to reproduce 113 and 85 cm^{-1} frequencies of the oscillations, γ_i/μ_i are the damping rates and $k_{D\Sigma}$ is the coupling between the two modes. A numerical fit of the oscillating part of the time dependent data[12] with these equations of motion gives the time evolution of the oscillating components D_{osc}(t) and Σ_{osc}(t) (Fig. 3(g)). These curves reproduce well the initial activation of the 113 cm^{-1} breathing oscillation, in agreement with the displacive description of the ISC along D. The fit also evidence a very fast damping of the breathing mode within 166 fs (γ_D/μ_D=6ps^{-1}). These results are in agreement with the theoretical model[8] introduced above, which considers an ISC of tens of femtoseconds accompanied by a structural elongation of the order of 100–200 fs and a damping time constant shorter than the period of the breathing mode (300 fs here). The observed delayed coherent activation of Σ characterizes the energy transfer from the breathing to the bending modes schematically represented in Fig. 4b and the smaller damping of the bending mode (γ_Σ/μ_Σ=1.16 ps^{-1}) indicates that the system oscillates (in the HS potential) as it gets vibrationally cooled within 900 fs. The additional transfer to other modes, for instance to lower frequency optical lattice phonons, can also be considered. A lattice mode is observed at 33 cm^{-1} (Fig. 3d), but its spectral weight is weaker. Thus, the major part of energy of the absorbed photon (1.9 eV) is dissipated, since each coherent molecular phonon only accounts for a small fraction of that energy. For instance, the energy of the breathing mode, E=½ $m\omega^2D^2$, can be estimated to only 40 meV, with reduced mass m=8.5 amu, angular frequency ω=2π*113cm^{-1} and elongation D≈0.2Å.

Conclusion.– In the emerging field of control science, understanding the physical processes allowing functionalization with light on ultrafast time scale is a key issue. Our results confirm the fast intersystem crossing observed in such transition-metal systems[23-28], as the change of electronic state is shorter than 50 fs and followed by a significant metal-ligand elongation within 160 fs. This initial structural change is directly coupled to the change of electronic state because of the less bonging nature of the HS state. Our experimental studies more importantly provides an experimental demonstration that the fast and highly efficient ISC is driven by the dephasing of the photoexcited state into the HS phonon states. The activated breathing mode is damped on a timescale (160 fs) close to its half-period, which allows an efficient trapping in the HS state as the decrease of the oscillation amplitude hinders recurrence to the initial state. We also show that the molecular bending is involved too, since the Fe-N elongation once established triggers the increase of the N-Fe-N bending because of ligand rigidity. Its delayed activation reveals a curved trajectory on a multi-dimensional potential energy surface, which underlines the limits of conventional descriptions along a single breathing coordinate on potential energy curves. This description of the photoswitching at the molecular scale, accompanied by important energy redistribution, sets the initial conditions for the slower transformation at material scale [35,36]. Such combination of x-ray and optical spectroscopies is key to disentangle the role of different degrees of freedom of electronic and/or structural nature in photoinduced phenomena.

This work was supported by the Institut Universitaire de France, Rennes Métropole, Région Bretagne (CREATE 4146), ANR (ANR-13-BS04-0002), CNRS (PEPS SASLELX) and Europe (FEDER). Portions of this research were carried out at the Linac Coherent Light Source (LCLS) at SLAC National Accelerator Laboratory. LCLS is an Office of Science User Facility operated for the U.S. Department of Energy Office of Science by Stanford University.

1 K. Nasu, Ed., *Photoinduced phase transitions* (Ed. World Scientist, Singapore, 2004).
2 V. S. Petrovic *et al*, *Phys. Rev. Lett.* **108**, 253006 (2012).
3 D. Polli *et al*, *Nature* **467**, 440–443 (2010).
4 H. Uemura, H. Okamoto. *Phys. Rev. Lett.* **105**, 258302 (2010).
5 M. Gao *et al*, *Nature* **496**, 343-346 (2013).
6 A. Kirilyuk, A.V. Kimel, T. Rasing. *Rev. Mod. Phys.* **82**, 2731–2784 (2010).
7 M. Halcrow, Ed., *Spin-crossover materials* (Wiley, West Sussex, 2013) ISBN 9781119998679.
8 M. van Veenendaal, J. Chang, A.J. Fedro. *Phys. Rev. Lett.* **104**, 067401 (2010).
9 J. Chuang, A.J. Fedro, M. van Veenendaal. *Phys. Rev. B* **82**, 075124. (2010).
10 E. König, K. Madeja. *Inorg. Chem.* **6**, 48 (1967).
11 E.W. Müller, H. Spiering, P. Gütlich. *Chem. Phys. Lett.* **93**, 567 (1982).
12 The supplementary materials contains information on the X-ray structure analysis, the pump-probe methods, computations of the density of state and molecular dynamics and coupled oscillator model. Video S1 shows the breathing mode and video S2 the ligand bending mode of [Fe(phen)2(NCS)2].See Supplemental Material [url], which includes Refs. [13-18].
13 J.A. Real, B. Gallois, T. Granier, F. Suez-Panama, J. Zarembovitch. *Inorg. Chem.* **31**, 4972 (1992).
14 P. Ganguli, P., Gütlich, P. & Mûller, E. W. Effect of Metal dilution on the Spin-crossover behavior on $[Fe_xM_{1-x}(phen)_2(NCS)_2]$. *Inorg. Chem.* **21**, 3429-3433 (1982).
15 Frisch, M. J. *et al*, GAUSSIAN03 (revision C.02), Gaussian, Inc., Wallingford CT, 2004.
16 S. Matar, J.F. Létard. *Z. Naturforsch* **65b**, 565 – 570 (2010).
17 E. Jones, T. Oliphant, P. Peterson and others, SciPy: Open Source Scientific Tools for Python (2001-), http://www.scipy.org/.
18 http://wwwasdoc.web.cern.ch/wwwasdoc/minuit/minmain.html
19 M. Marchivie *et al*, *J. Am. Chem. Soc.* **124** 194-195. (2002).
20 V. Briois *et al*, *J. Am. Chem. Soc.* **117**, 1019–1026 (1995).
21 M. Harmand *et al*, *Nat. Photonics* **7**, 215-218 (2013).
22 S. Matar, J.F. Létard. *Z. Naturforsch* **65b**, 565 – 570 (2010).
23 C. Bressler *et al*, Science **323**, 489-492 (2009).
24 N. Huse *et al*, *J. Phys. Chem. Lett.* **2**, 880-884. (2011).
25 H.T. Lemke, *et al*, *J. Phys. Chem. A* **117**, 735-740 (2013).
26 C. Consani *et al*, *Angew. Chem. Int Ed.* **121**, 7320 (2009).
27 W. Gawelda *et al*, *J. Am. Chem. Soc.* **129**, 8199–8206 (2007).
28 M. Chergui in *Spin-crossover materials*, M. Halcrow, Ed. (Wiley, West Sussex, 2013) ISBN 9781119998679.
29 G. Baranovic, D. Babic. *Spectrochem. Acta A* **60**, 1013. (2004).
30 K.L. Ronayne *et al*, *Phys. Chem. Chem. Phys.* **8**, 4685 (2006).
31 M. Buron-Le Cointe *et al*, *Phys. Rev. B* **85**, 064114 (2012).
32 A. Hauser *et al*, *Coord. Chem. Rev.* **250**, 1642-1652 (2006).
33 Y. Kawakami *et al*, *Phys. Rev. Lett.* **103**, 066403. (2009).
34 M. Först *et al*, *Nature Phys.* **7**, 854 (2011).
35 M. Lorenc *et al*, *Phys. Rev. Lett.* **103**, 028301 (2009).
36 M. Lorenc *et al*, *Phys. Rev. B.* **85**, 054302 (2012).

Supplemental Material for

Sequential activation of molecular breathing and bending during spin-crossover photoswitching revealed with femtosecond optical and x-ray absorption spectroscopy

Marco Cammarata,[1] Roman Bertoni,[1] Maciej Lorenc,[1] Hervé Cailleau,[1] Sergio Di Matteo,[1] Cindy Mauriac,[2] Samir Matar,[2] Henrik Lemke,[3] Matthieu Chollet,[3] Sylvain Ravy,[4] Claire Laulhé,[4] Jean-François Létard,[2] Eric Collet,[1,*]

* To whom correspondence should be addressed. E-mail: eric.collet@univ-rennes1.fr

[1] *Institut de Physique de Rennes, UMR CNRS 6251Université Rennes 1, 35042 Rennes cedex, France.*

[2] CNRS, Université de Bordeaux, ICMCB, 87 avenue du Dr. A. Schweitzer, Pessac, 33608 France.

[3] *LCLS, SLAC National Laboratory, Menlo Park, CA, USA.*

[4] Synchrotron SOLEIL, L'Orme des Merisiers, Saint Aubin, 91192 Gif-sur-Yvette France.

Content:

1 Samples:

Single crystals of $[Fe(phen)_2(NCS)_2]$ compound were obtained by slow diffusion as indicated in reference *(13)*. The powder films of $[Fe(phen)_2(NCS)_2]$ compound have been prepared according to the description of Gütlich and co-workers *(14)*; i.e. i) by reacting 0.77 g (2.77 mmol) of $FeSO_4 \cdot 7H_2O$ and 0.539 g (5.55 mmol) of KSCN in dry and freshly distilled methanol (6 ml), ii) by filtered off the K_2SO_4 precipitate, and iii) by adding the solution to 1 g (5.55 mmol) of 1,10-phenanthroline in 3 ml of methanol. The red precipitate was filtered off, washed with methanol and diethyl ether and further purified by the Soxhlet technique during 48 hours corresponding to the form I of $[Fe(phen)_2(NCS)_2]$ showing a first order spin transition around 180 K and LIESST, confirmed by magnetic measurements shown in Fig. S1. The powder film consists in µm size crystals in a polymeric matrix. XANES spectra measured on single crystal or on powder film are very similar. Fig. 1B shows the XANES spectra for the LS (140 K) and HS (200 K) states measured on the powder film.

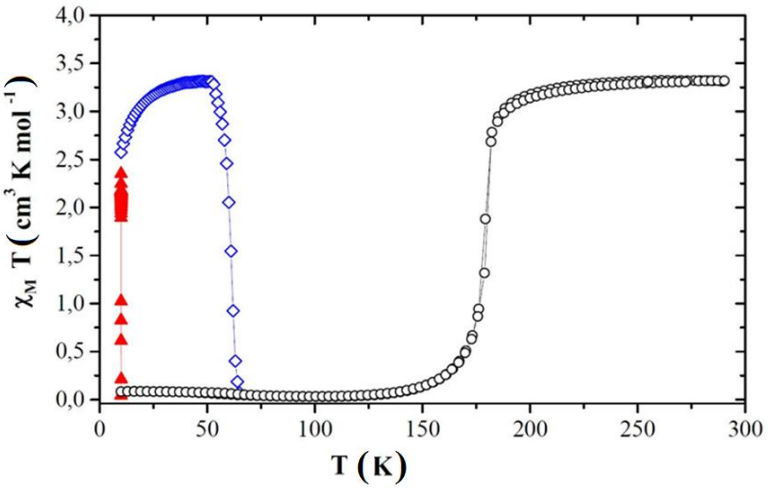

Figure S1. Magnetic (black) and photomagnetic (colored properties of a polycrystalline sample of $[Fe(phen)_2(NCS)_2]$. Light excitation was performed at 650 nm.

2 X-ray structure analysis of thermal LS to HS phase transition.

Structural investigations at thermal equilibrium in the 100-250 K range were performed by X-ray diffraction on single crystals. Data were collected on a four-circle Oxford Diffraction Xcalibur 3 diffractometer (MoK_α radiation) with a 2D Sapphire 3 CCD detector, on samples with typical sizes around 200 × 150 × 50 μm^3. The single crystals of form I were mounted in an Oxford Cryosystems nitrogen-flow cryostat. The structural refinements gave similar results as the ones already reported in the literature *(see ref 19 in the letter)*, allowing to follow the evolution of the main structural changes around the coordination sphere of the Fe atom are shown in Fig. S2:

- the distances between the Fe and the bonded N atoms (there are 2 Fe-N_{phen} and 1 Fe-N_{NCS} independent bonds) and the average: $< Fe-N >= \frac{1}{6}\sum_{i=1}^{6} Fe-N_i$

- the distortion Σ of the FeN_6 octahedron is measured by the sum of the deviation from 90° of the 12 N-Fe-N cis ϕ angles in the coordination sphere: $\sum = \sum_{i=1}^{12} |90 - \phi_i|$

In the LS phase $\langle Fe\text{-}N\rangle_{LS} \approx 1.97$ Å and $\Sigma_{LS} \approx 35°$ and these parameters discontinuously change in the HS phase to $\langle Fe\text{-}N\rangle_{HS} \approx 2.16$ Å and $\Sigma_{HS} \approx 65°$. This discontinuous change of the structure is related to the discontinuous change of the spin state of $[Fe(phen)_2(NCS)_2]$ and illustrate that structure and electronic states are strongly coupled.

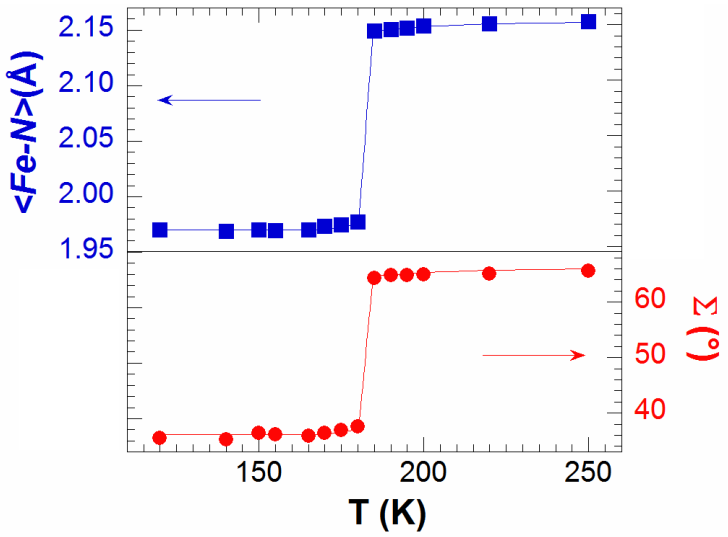

Figure S2. Temperature dependence of Fe-N bonds and Σ parameter, showing the first-order phase transition around 180 K between LS and HS states.

3 Experimental details of femtosecond pump-probe studies

We have investigated the LS-to-HS photoswitching dynamics by performing pump-probe measurements at 140 K, where $[Fe(phen)_2(NCS)_2]$ is in the pure LS state. The sample was cooled by a nitrogen cryostream. For x-ray and optical studies, the pump wavelength was set to 650 nm where it efficiently induces LS-to-HS transition through MLCT process (see also Fig. S1 & S6).

3.1 x-ray absorption probe:

Optical pump and x-ray probe studies were performed at the XPP beamline of the LCLS X-FEL. A femtosecond laser operating at 120 Hz delivered 50 fs pump pulses at 650 nm focused to 500×500 μm^2 on the sample, with intensities of the order of 2-5 µJ. The x-ray beam was monochromatised using the XPP double Si(111) crystal monochromator. To ensure pulse durations limited time resolution and avoid thermal drifts of the timing, the recently developed "timing tool" has been used *(see ref 21 in the letter)*. This has the capability of measuring the relative arrival time between x-ray and infrared laser pulses with few tens of femtoseconds resolution and on a shot-to-shot basis. The x-ray fluorescence was collected using a Si diode (Canberra FD450-18-300RM) positioned horizontally at a 90° angle with respect to the x-ray beam propagation direction. The incoming intensity was measured using noninvasive diagnostics (after the x-ray monochromator) developed for pulsed x-ray radiation. We detected the total x-ray fluorescence yield to obtain the XANES spectra in the vicinity of the Fe K-edge (7.120 keV). Optical pump - XAS probe studies on single crystal gave weak signal because of the limited matching of the penetration depths of optical pump and x-ray probe. Therefore, we used the powder films (~few centimeters square) and yet thin (5 µm) samples for increasing the signal/noise ratio.

3.2 Optical probe:

The spin-state switching is associated with important changes of optical properties of the $[Fe(phen)_2(NCS)_2]$ crystals. Absorption and reflectivity spectra are shown in Fig. S3 for the LS (100 K) and HS (210 K) states. The MLCT band of the LS state is centered around 650 nm, the wavelength used as a pump, whereas the d-d band is around 760 nm. The spectra are not very structured and the LS to HS thermal conversion results in a global increase of absorption and decrease of reflectivity below 670 nm and above 720 nm, as illustrated by the temperature dependence of optical transmission at 900 nm.

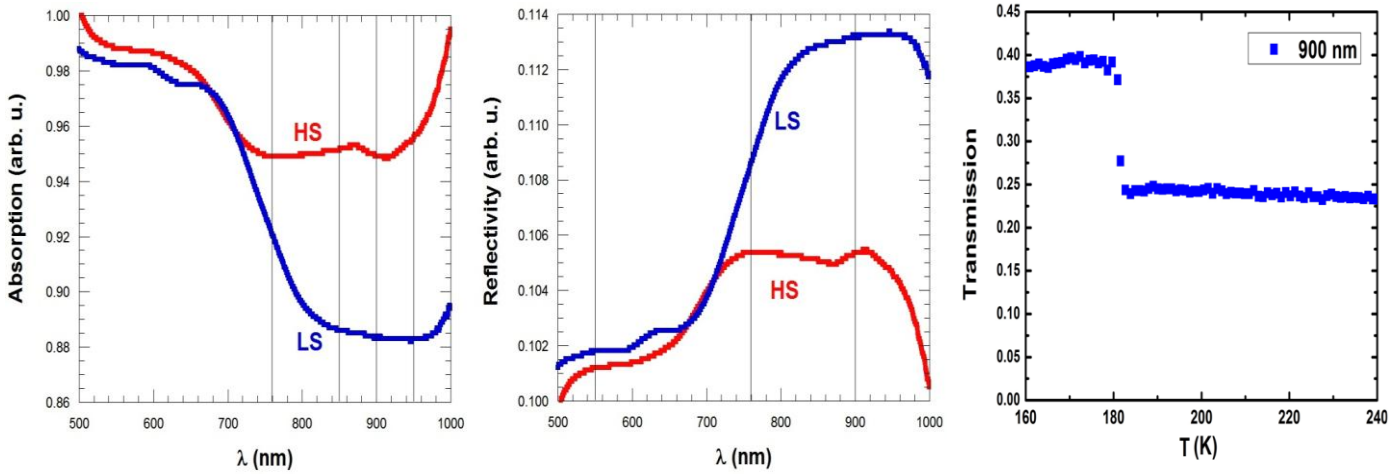

Figure S3. optical absorption (left) and reflectivity (middle) spectra measured in the LS (100 K) and HS (210 K) states. The wavelengths used for time-resolved transmission and reflectivity measurements are indicated by the vertical lines. Temperature dependence of transmission at 900 nm (right).

Optical pump-probe studies were performed in Rennes, with a wavelength tunable femtosecond laser operating at 1 kHz and delivering 50 fs pump and probe pulses. Two-colour pump-probe spectroscopy studies were performed on single crystals (10-20µm thick). Time-resolved reflectivity measurements were performed at 550, 760 and 900 nm. Time-resolved transmission measurements were performed at 760, 850, 900 and 950 nm, since the absorption is too high in the visible range. A typical measurement of transient optical density (OD) at 900 nm is presented in Fig. S4.

Single-wavelength measurements probed the resulting dynamics through changes of optical reflectivity (OR) and optical transmission (OT) of the single crystal. In addition to data presented in Fig. 2 we show in Fig. S4 OT data at 760 nm and 950 nm (A&D) and their oscillating component (B&E). The time-dependent FFT (C&F) were obtained by sliding a 700 fs width Gaussian window. The Fe-N breathing mode at 113 cm^{-1} (with 300 fs period) observed at 760 nm is observed just after excitation, whereas the mode observed at 950 nm, corresponding to the bending mode also observed in Fig. 3 is activated later. FFT of the oscillating component of time-dependent optical spectroscopy indicate that mainly the breathing and bending modes are observed in the time-dependent data.

The time dependent OR and OT data are fitted with:

$$OR(t) = [1 - exp(-(t - t_0)/\tau)] * G(t - t_0,\sigma) \text{ and } OT(t) = exp(-(t - t_0)/\tau) * G(t - t_0,\sigma)$$

where τ is the exponential population of the HS state and σ is the overall 140 fs instantaneous response function (IRF) of this experiment.

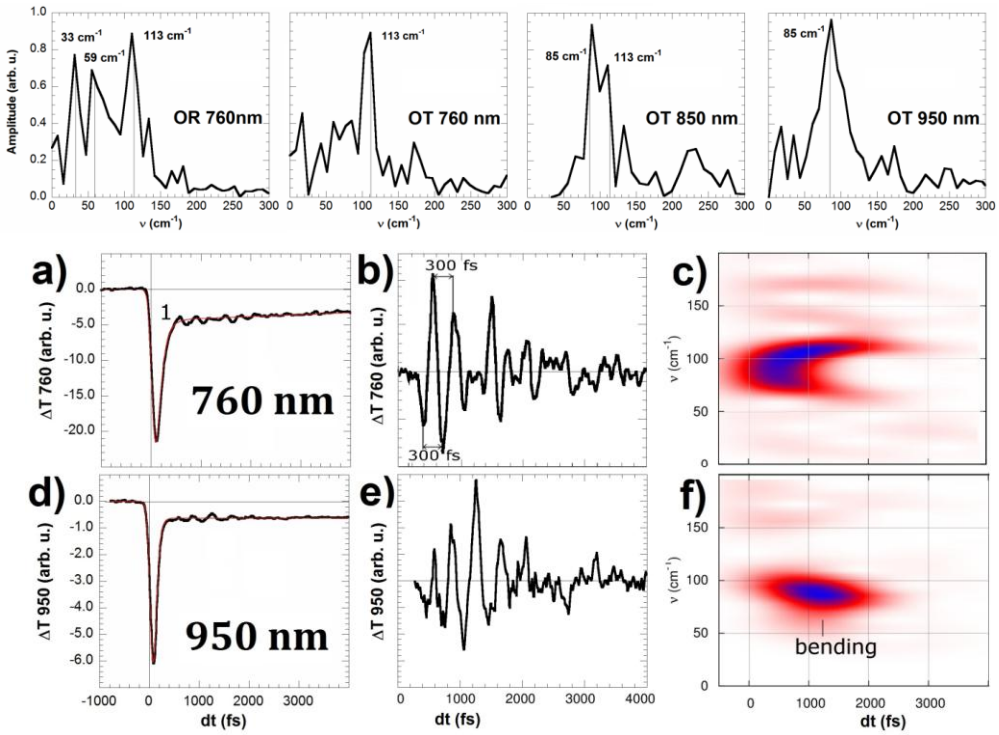

Figure S4. OT at 760 nm (A), oscillating component (B) with ≈300 fs period (ν=113 cm^{-1}) mode and time-dependent FFT showing the 113 cm^{-1} mode (C). OT at 950 nm (D), oscillating component (E) with a 85 cm^{-1} mode and time-dependent FFT (F)**.** FFT of OR at 760 nm and OT at 760, 850 and 950 nm are shown below and indicate the two main modes at 113 cm^{-1} (breathing) and 85 cm^{-1} (bending).

4 Solid-state Computations of the density of state and molecular dynamics:

Density Of State (DOS) calculations were already performed for in the LS phase of $[Fe(phen)_2(NCS)_2]$ and detailed presentation is given in ref *(16)*. The same method was used here for comparing the change of DOS in the HS phase. Results are given in Fig. S5. The major feature is the low dispersion of the peaks which is descriptive of a molecular system, *i.e.* in opposition to a metal or an intermetallic system where the DOS are broadened. Somehow, even in the organized periodic solid state, $[Fe(phen)_2(NCS)_2]$ exhibits a molecular behavior. The key information regarding the time-resolved optical studies presented here is that on both sides of the gap the DOS correspond the Fe *d* states which are respectively t_{2g}- and e_g-like , as indicated by the colored bands. The DOS calculations indicate that

- in the LS state the t_{2g}-e_g gap is around 1.9 eV
- in the HS state the t_{2g}-e_g gap is around 1.6 eV

The LMCT process induced by femtosecond excitation in the LS state is shown by the red arrow.

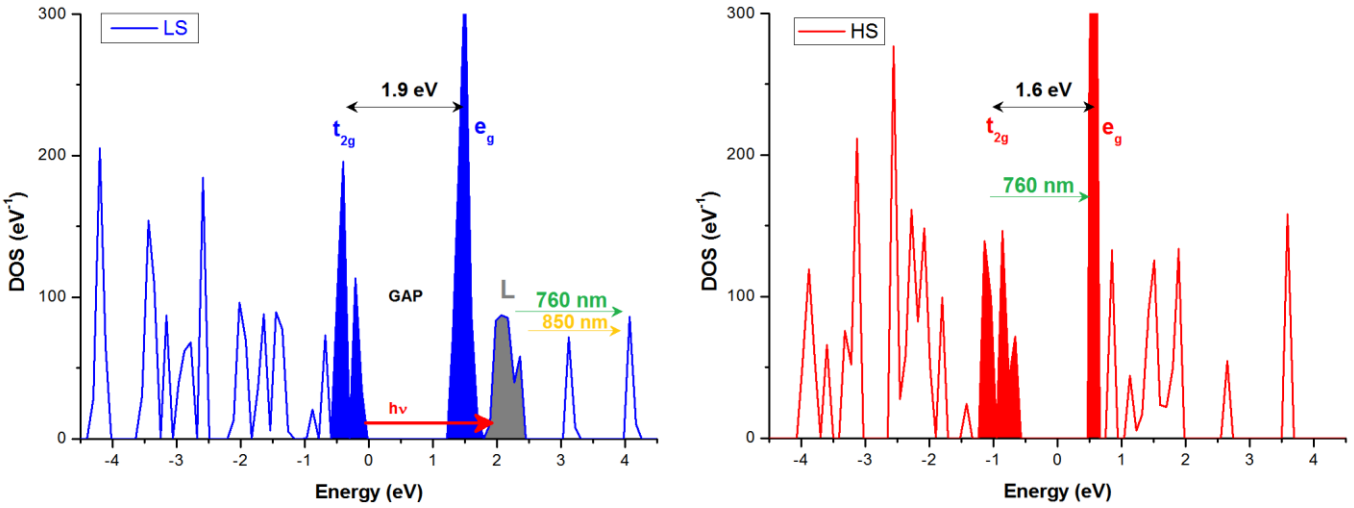

Figure S5. Total DOS for $[Fe(phen)_2(NCS)_2]$ in its LS (blue) and HS (red) states with the t_{2g} and e_g like bands (colored). Is the LS state (left) two nearly degenerates e_g like bands are 1.9 eV above the t_{2g}. The light excitation (hν red arrow) generates metal-to-ligand charge-transfer from metal (t_{2g}-like) to ligand (L-like) states (MLCT). The photoexcited *L* state gives rise to absorption peak around 760-850 nm (arrows left). In the HS state the main absorption around 760 nm is the t_{2g}-e_g transition.

The LUMO (lowest unoccupied molecular orbitals) lying ≈ 2 eV above the LS HOMO (highest occupied molecular orbital) orbitals with paired electrons, are shown in Fig. S6 and have electron density on the phen groups only. The HS t_{2g}-like orbital of lower energy is of ionic character and shows electron density mainly on the Fe-N_{NCS} bonds (Fig. S6).

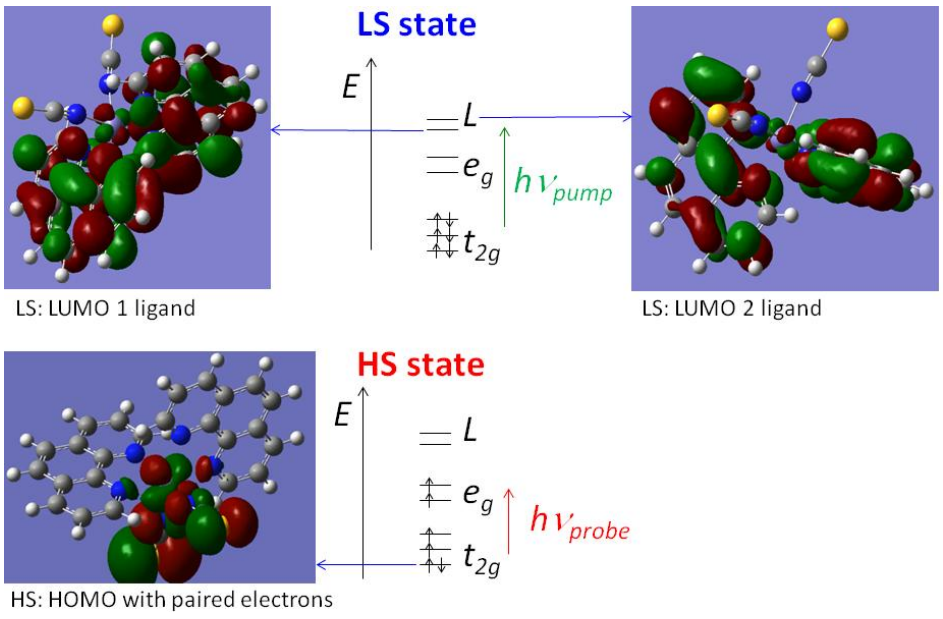

Figure S6. Schematic energy diagram and molecular orbitals obtained from DFT calculation. The LS LUMO molecular orbitals L of the ligand indicates that the laser pump induces a MLCT process from t_{2g} to L occurs on the phen groups. The HS HOMO with paired electron corresponds to the Fe-N_{NCS} bonds and the probe signal is modulated by the t_{2g}-e_g splitting. Fe atom is in the center, N atoms are blue, C atoms are grey, S atoms are yellow, H atoms are white.

Molecular vibration frequencies calculations were carried out for $[Fe(phen)_2(NCS)_2]$ after geometry optimization, by using hybrid B3LYP functional with LANL2DZ basis set within Gaussian09 code *(15)*. Frequencies are determined from the second derivatives of the energy with respect to the atomic positions and then operating transformation to mass-weighted coordinates. Exploring the results especially for the vibrations and their animations with screen captures was done with Gaussview annex module to Gaussian. Video S1 shows the breathing mode and video S2 show the ligand bending mode. A complete analysis will be published elsewhere.

5 Coupled oscillators model:

The motion of two elastically coupled oscillators are described by the classical equations of motions:

$$\begin{cases} \mu_D \ddot{D} + \gamma_D \dot{D} + k_D D + k_{D\Sigma}(D - \Sigma) = 0 \\ \mu_\Sigma \ddot{\Sigma} + \gamma_\Sigma \dot{\Sigma} + k_\Sigma \Sigma - k_{D\Sigma}(D - \Sigma) = 0 \end{cases}$$

$k_{D\Sigma}$ is the coupling between the two modes *D* and Σ, γ_i the damping constants due to the coupling to the phonon bath, μ_i the reduced masses. The frequencies of the modes are $\nu_i = \frac{1}{2\pi}\sqrt{\frac{k_i}{\mu_i}}$.

Given a set of constants $\mu_i, \gamma_i, k_i, k_{D\Sigma}, i = D, \Sigma$ and initial conditions:

$D(t=0), \dot{D}(t=0),\ \Sigma(t=0),\ \dot{\Sigma}(t=0)$

numerical integration (using the python module *scipy.integrate.odeint (17)*) yields the displacements of *D* and Σ as function of time. The model functions S^{900nm} in Fig. 4B and S^{850nm} in Fig. 4C of the measured signals y^{900nm} and y^{850nm} are then build as

$$\begin{cases} S^{900nm}(t) = a1_\Sigma * \Sigma(t) \\ S^{850nm}(t) = a2_D * D(t) + a2_\Sigma * \Sigma(t) \end{cases}$$

The model functions allow to define a like hood function as follows

$$\chi^2 = \sum [(S^{900nm}(t_i - t_0) - y_i^{900nm})/\sigma]^2 + \sum \left[\left(S^{850nm}(t_j - t_0) - y_j^{850nm}\right)/\sigma\right]^2$$

This function has been minimized using the Minuit library *(18)* on the data in the time interval [0.2:2.5] ps. The results together with the 1-standard-deviation error bars are reported in the table S1 hereafter.

Since the relations displacements/change of optical density are unknown, $a1_\Sigma$, $a2_D$, $a2_\Sigma$ are in arbitrary units as well as the amplitudes *D* and Σ. In our analysis the reduced masses (μ_D = 8.5 AMU, μ_Σ= 6 AMU) of the oscillators *D* and Σ were obtained from the *Gaussian* calculations. The only parameters with physical dimensions are the damping rates γ_i/μ_i of the oscillators.

The fit gives ν_D =113cm^{-1} and ν_Σ =85cm^{-1}.

Table S1. Results and standard-deviation of the fit of the motion of two elastically coupled oscillators.

Parameter	Unit	Best Fit	error bar
γ_D/μ_D	ps^{-1}	6.2	0.25
γ_Σ/μ_Σ	ps^{-1}	1.16	0.1
k_D	$AMU.ps^{-2}$	4050	60
k_Σ	$AMU.ps^{-2}$	1570	8
$k_{D\Sigma}$	$AMU.ps^{-2}$	29.3	0.3
$a1_\Sigma$	arbitrary	$2.6\cdot10^{-3}$	$0.1\cdot10^{-3}$
$a2_\Sigma$	arbitrary	$3.2\cdot10^{-3}$	$0.2\cdot10^{-3}$
$a2_D$	arbitrary	$6.8\cdot10^{-5}$	$0.3\cdot10^{-5}$
t_0	ps	-0.13	0.002
$D(t=0)$	arbitrary	-8.4	1.5
$\dot{D}(t=0)$	arbitrary	1072	12
$\Sigma(t=0)$	arbitrary	1.62	0.04
$\dot{\Sigma}(t=0)$	arbitrary	-9.0	0.6

References :

13 J.A. Real, B. Gallois, T. Granier, F. Suez-Panama, J. Zarembovitch. *Inorg. Chem.* **31**, 4972 (1992).

14 P. Ganguli, P., Gütlich, P. & Mûller, E. W. Effect of Metal dilution on the Spin-crossover behavior on $[Fe_xM_{1-x}(phen)_2(NCS)_2]$. *Inorg. Chem.* **21**, 3429-3433 (1982)

15 Frisch, M. J. *et al*, GAUSSIAN03 (revision C.02), Gaussian, Inc., Wallingford CT, 2004.

16 S. Matar, J.F. Létard. *Z. Naturforsch* **65b**, 565 – 570 (2010).

17 E. Jones, T. Oliphant, P. Peterson and others, SciPy: Open Source Scientific Tools for Python (2001-), http://www.scipy.org/

18 http://wwwasdoc.web.cern.ch/wwwasdoc/minuit/minmain.html